International Journal of Nanomedicine

Dovepress

open access to scientific and medical research

Open Access Full Text Article

ORIGINAL RESEARCH

Synergistic Combination of an Intelligent Nanozyme and Radiotherapy for Treating Renal Cancer

Lei Lei, Ke Wang

Henan Provincial Chest Hospital, Zhengzhou, 450008, Henan, People's Republic of China

Correspondence: Ke Wang, Email 13837178129@163.com

Background: Preserving nephrons while avoiding tumor recurrence during the treatment of renal cell carcinoma remains as a challenge in clinic. To achieve desired therapeutic outcome, we developed specific nanozymes based on the tumor microenvironment and evaluated its efficacy in combination with radiotherapy.

Methods: Herein, a hybrid nanozyme CeO_2@Au-PEG nanocomposite nanoparticle (NPs) was developed for the treatment of renal tumor. It was composed of gold nanozyme decorated CeO_2 nanorods and exhibited both glucose-oxidase like by gold nanozyme and peroxidase-like catalytic activities. Due to the high metabolic rate of tumor cells, they take up a huge amount of glucose to survive and proliferate. Therefore, we generated CeO_2@Au-PEG NPs, which exhausted glucose in the tumor tissue and generated hydrogen peroxide, depleting the source of energy and causing tumor cell death. Then the generated hydrogen peroxide was degraded by the peroxidase-mimicking properties of CeO_2@Au-PEG NPs, elevating oxidative stress and thus enhancing tumor cell death. Moreover, due to the high mass nuclei of gold and cerium, they could further sensitize the tumors to radiotherapy and thus thoroughly eliminate tumors.

Results: With enough biocompatibility, CeO_2@Au-PEG NPs showed superior ability to deplete glucose as well as enhance oxidative stress by producing reactive oxygen species in RENCA cells under ionizing irradiation. Moreover, CeO_2@Au-PEG NPs greatly improved radiotherapy mediated tumor ablation in tumor bearing mice.

Conclusion: Systematic experiments demonstrated the synergistic therapeutic effects of the combination of CeO_2@Au-PEG NPs and radiotherapy in renal tumor model, which may serve as a promising strategy for treating renal cancer patients in the clinic.

Keywords: nanozyme, radiotherapy, glucose consumption, reactive oxygen species, renal cell carcinoma

Introduction

According to the cancer statistics estimated in 2023, the incidence rate of tumors in the urinary system ranked among the top ten cancers.[1] Among all the estimated cases of urinary cancer, cancers occurring in the kidney and renal pelvis account for one-third of new diagnoses with renal cell carcinoma accounting for 90% of the cases with kidney cancer.[2] Surgery including partial nephrectomy as well as radical nephrectomy is widely performed during the treatment of renal cell carcinoma patients.[3,4] Targeted therapies utilizing chemotherapeutic drugs and immunotherapy are being utilized as strategies for systemic therapy.[5] However, it is necessary to preserve as much nephron as possible during the treatment of renal cell carcinoma since the kidney plays an important role in the excretion of waste from the body. Meanwhile, incomplete clearance of cancer cells might lead to tumor recurrence.[6,7] Therefore, to improve the patient's quality of life as well as inhibit tumor recurrence, researchers are exploring nanocomposites, which can specifically respond to the tumor microenvironment (TME) or can be tailored according to the tumor characteristics.[8–10] The introduction of nanocomposite promotes tumor ablation without impairing kidney function, suggesting its promising potential for treating renal cell carcinoma patients.

Compared to normal tissues, tumor tissues with high metabolism tend to consume more glucose. Due to this, glucose oxidase (GOx) which catalyzes the conversion of glucose and oxygen to gluconolactone and hydrogen peroxide has gained increasing attention in the nanomedicine field.[11–14] The energy depletion caused by these enzymes, and the release of hydrogen peroxide (H_2O_2) cause tumor cell death. In a recent study, tri-metal nanospheres decorated with glucose oxidase termed AuPtAg-GOx were engineered for synergistic tumor therapy via starvation therapy and photothermal therapy to

Received: 15 May 2023
Accepted: 2 November 2023
Published: 22 January 2024

augment immunotherapy efficacy. Under laser irradiation, the glucose depletion efficiency of AuPtAg-GOx was augmented, which enhanced the therapeutic outcome.[15] Zhang et al reported a $MnSiO_3$@Met@GOx nanocomposite that could be triggered in mild-acidic pH and GSH overexpressing TME. H_2O_2 derived from glucose in the presence of the nanocomposite was converted to toxic hydroxyl radicals (OH) by decomposed Mn^{2+}, leading to cell death and tumor ablation.[16] To effectively inhibit glioma tumor recurrence after surgery, Li et al developed a sprayed gel containing GOx@MnCaP nanoparticles (NPs), which improved the therapeutic outcome. GOx decomposes glucose to produce H_2O_2, which is then converted to cytotoxic reactive oxygen species (ROS) by Mn^{2+} to induce tumor cell apoptosis and suppress proliferation.[17]

Recently, enzyme mimicking nanocomposites termed nanozymes are extensively being investigated.[18–20] Compared with natural enzyme, these nanozymes possess advantages such as physiological stability, suitability for mass production and high catalytic efficiency.[21,22] Numerous nanozymes have been applied for treating cancers, owing to their catalase, superoxide dismutase, peroxidase (POD) or oxidase mimicking properties.[23–25] Specifically, with high accumulation of H_2O_2 in the TME, nanozymes with peroxidase-mimicking property are capable of turning these H_2O_2 molecules into cytotoxic ROS, killing tumor cells. According to Dong et al, CaF_2 nanozyme was synthesized to enable Ca^{2+} release and ROS generation from ultrasonic (US) amplified POD-catalytic activity, which promoted Ca^{2+} overload and mitochondrial dysfunction. This strategy, based on CaF_2 nanozyme, showed enhanced ability to kill both breast tumor and liver tumor upon US exposure.[26] A titanium nitride-based nanoparticle termed TLGp was reported by Liu et al for photo-enhancing POD catalytic activity. GOx in TLGp produced abundant H_2O_2, which was then converted to ROS to achieve tumor therapy while minimizing side effects.[27] In addition, Nan et al reported iron phthalocyanine-based Fe (II) Pc-A for cascade reaction, including POD, CAT and OXD activities, where H_2O_2 was decomposed to ROS to enhance oxidative stress in cancer cells and to realize multi-modal cancer therapy.[28]

Ionizing irradiation is widely used for suppressing tumor growth and elimination of tumors. To completely ablate tumor tissues while protecting normal tissues and augment radiotherapy (RT) efficacy, numerous noble elements have been utilized to design nanoplatforms.[20,29,30] Here, we constructed a novel nanozyme (CeO_2@Au-PEG) by decorating gold nanozyme on CeO_2 nanorods and then modified this nanocomposite with PEG. Under X-ray irradiation, energy deposited on both gold and cerium was enhanced, which further enhanced anti-tumor therapeutic efficacy of RT. Notably, although there is excessive amount of H_2O_2 in the TME compared with normal tissues, the ROS generated with the assistance of POD-mimicking nanozymes may not thoroughly eliminate tumor cells, leaving the possibility for tumor recurrence. Considering that abundant H_2O_2 is produced via the process of glucose oxidization, this nanozyme was designed to possess dual-catalytic properties including glucose-depletion as well as POD-mimicking activity (Scheme 1). In other words, it could produce sufficient H_2O_2 from intracellular glucose, which deprived cancer cells of the nutrients. Next, the generated H_2O_2 was decomposed into toxic ROS, inducing tumor cell death. Both in vitro and in vivo experiments demonstrated that the nanocomposites possessed desired biocompatibility, and that CeO_2@Au-PEG not only converted intracellular glucose into ROS by dual-catalytic properties, but also enhanced the cellular damage caused by ionizing radiation during RT to achieve highly efficient therapeutic outcome against renal cell carcinoma.

Results and Discussion

Preparation and Characterization of CeO_2@Au-PEG

The preparation of CeO_2@Au-PEG consisted of three steps, including the synthesis of porous CeO_2 nanorods with precursor of $Ce(NO_3)_3 \cdot 6H_2O$ and NaOH, loading of gold nanozyme on CeO_2 nanorods to obtain CeO_2@Au nanorods and decoration of polyethylene glycol (PEG) on nanorods to obtain CeO_2@Au-PEG nanocomposite (Figure 1a). As shown in Figure 1b, CeO_2 displayed the morphology of nanorods with a length of approximately 90 nm. CeO_2@Au was found to be composed of gold nanozyme coated around CeO_2 (Figure 1c). TEM images of Au-PEG were shown in Figure S1. Besides, the zeta potential of CeO_2, CeO_2@Au and CeO_2@Au-PEG were measured to be −11.5 mV, −21.0 mV and −23.0 mV, respectively. The change in zeta potential from −21.0 mV to −23.0 mV suggested the improved colloidal stability after PEGylation. After CeO_2@Au-PEG and Au-PEG were dissolved in phosphate buffered solution (PBS) for 24 h (Figure S2), the solution still remains uniform and clarified, demonstrating satisfied stability of CeO_2@Au-PEG and Au-PEG.

Next, X-ray diffraction (XRD) analysis was conducted to further confirm the structure of CeO_2 and CeO_2@Au. Several peaks corresponding to (1 1 1), (2 0 0), (2 2 0), (3 1 1), (2 2 2), (4 0 0) and (3 3 1) facets in XRD pattern of CeO_2 were identified

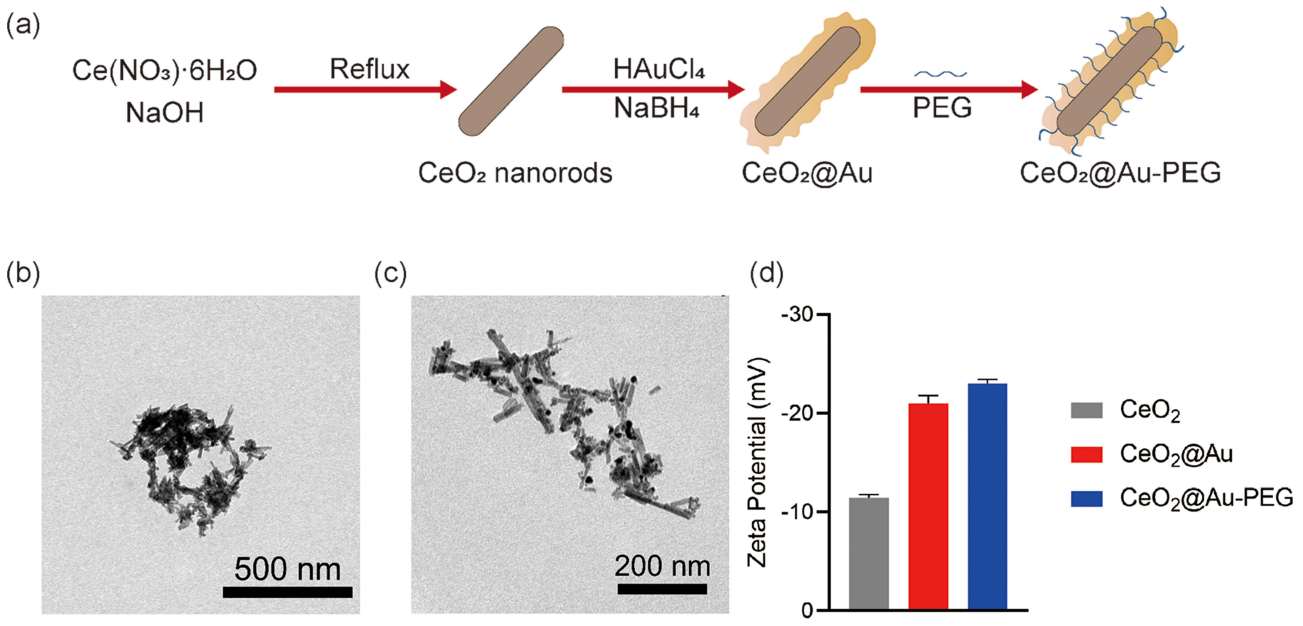

Figure 1 (**a**) Schematic illustration of the preparation of CeO_2@Au-PEG nanocomposite NPs, TEM images showing the morphology of (**b**) CeO_2 and (**c**) CeO_2@Au, (**d**) Zeta potential of CeO_2, CeO_2@Au and CeO_2@Au-PEG NPs.

as shown in Figure 2a. Diffraction peaks representing gold nanozyme including (1 1 1), (2 0 0), (2 2 0) and (3 1 1) crystal plane were observed in the XRD pattern of CeO_2@Au (Figure 2b). X-ray photoelectron spectroscopy (XPS) wide scan spectra of CeO_2 and CeO_2@Au are displayed in Figures S3 and 2c. It can be seen that cerium and oxygen were present in the obtained CeO_2. And XPS spectra of CeO_2@Au showed typical peaks including Ce 3d, O 1s and Au 4f, confirming the existence of cerium, oxygen and gold. Further investigation of high-resolution spectra of cerium from CeO_2 and CeO_2@Au are shown in Figures S4 and 2d, which possessed similar binding energy peaks. Typically, the Ce 3d spectra of CeO_2@Au showed five

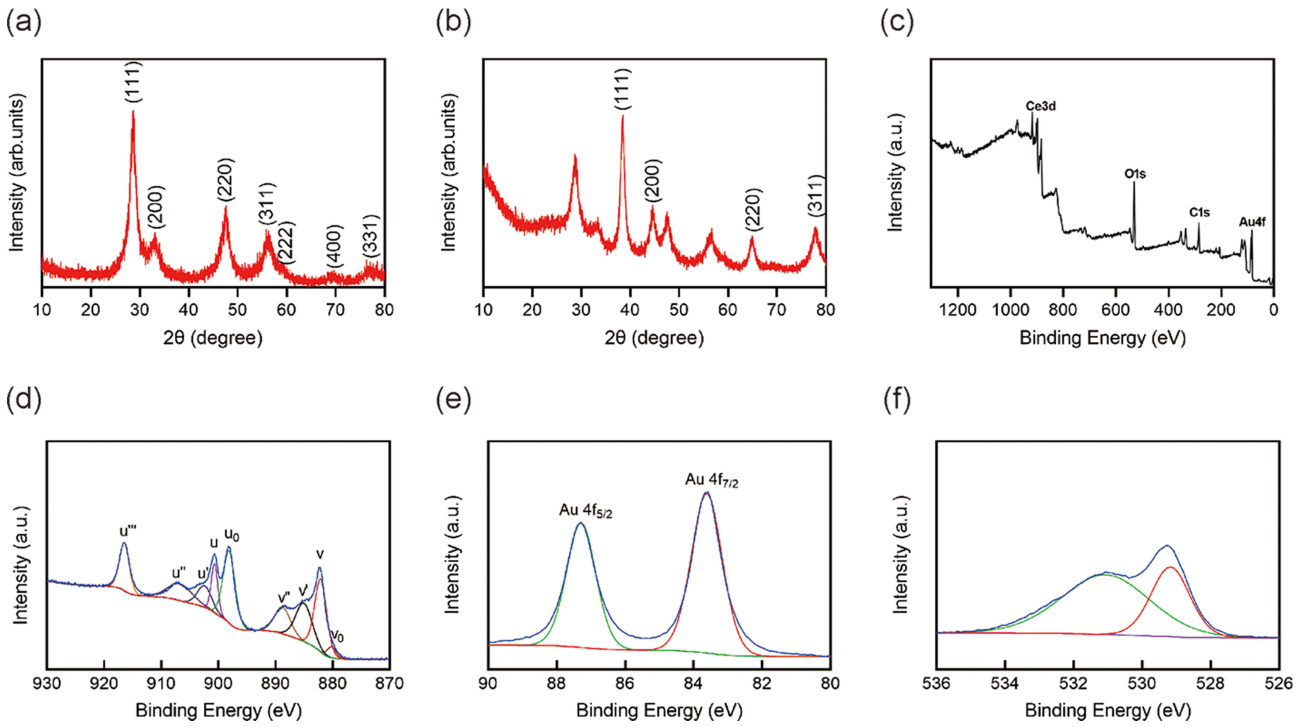

Figure 2 (**a** and **b**) XRD patterns of CeO_2 and CeO_2@Au NPs. (**c**) XPS analysis of CeO_2@Au NPs. (**d–f**) High-resolution XPS spectra of Ce 3d, Au 4f and O 1s.

peaks labeled u and five peaks labeled which can be attributed to $3d_{5/2}$ and $3d_{3/2}$ respectively. Moreover, the binding energy peaks of gold in the high-resolution spectra at 87.6 eV and 83.8 eV were attributed to $4f_{5/2}$ and $4f_{7/2}$ respectively. The binding energy peaks at 531.3 eV and 529.6 eV were designated to surface oxygen and lattice oxygen (Figure 2e). The above results thus demonstrated the successful fabrication of CeO_2@Au-PEG.

Evaluation of the in vitro Catalytic Activity of the Nanocomposite

Endowed with dual-catalytic properties, CeO_2@Au-PEG was internalized by cells, generating sufficient H_2O_2 from glucose, the primary source of cellular energy. Next, H_2O_2 was then converted to ROS by POD-mimicking properties of CeO_2@Au-PEG (Figure 3a). Ionizing irradiation caused significant damage in cells when treated in combination with CeO_2@Au-PEG. To evaluate these two reaction processes, both POD-mimicking catalytical activity and glucose consuming of CeO_2@Au-PEG were measured. The oxidation of glucose by gold nanozyme of CeO_2@Au-PEG can produce H_2O_2 and gluconic acid, resulting in a decrease in the pH value. As shown in Figure 3b, a reduction of pH values was seen as a consequence of gluconic acid generation, indicating the oxidation of glucose in the presence of CeO_2@Au-PEG. Moreover, an increase of H_2O_2 concentration was observed in the group treated with glucose + Au-PEG (Figure 3c). The POD-mimicking activity was also measured using 3, 3', 5, 5' - tetramethylbenzidine (TMB), which turned blue in the presence of ·OH. As shown in Figure 3d, typical absorption peaks at wavelength of 450 nm increased as the concentration of CeO_2@Au-PEG increased, which was due to the generation of ·OH by the catalytic activity of CeO_2@Au-PEG. The solution became more blue as concentration of CeO_2@Au-PEG increased. This confirmed that CeO_2@Au-PEG contributed to production of ·OH derived from H_2O_2, which was in turn generated upon the oxidation of glucose.

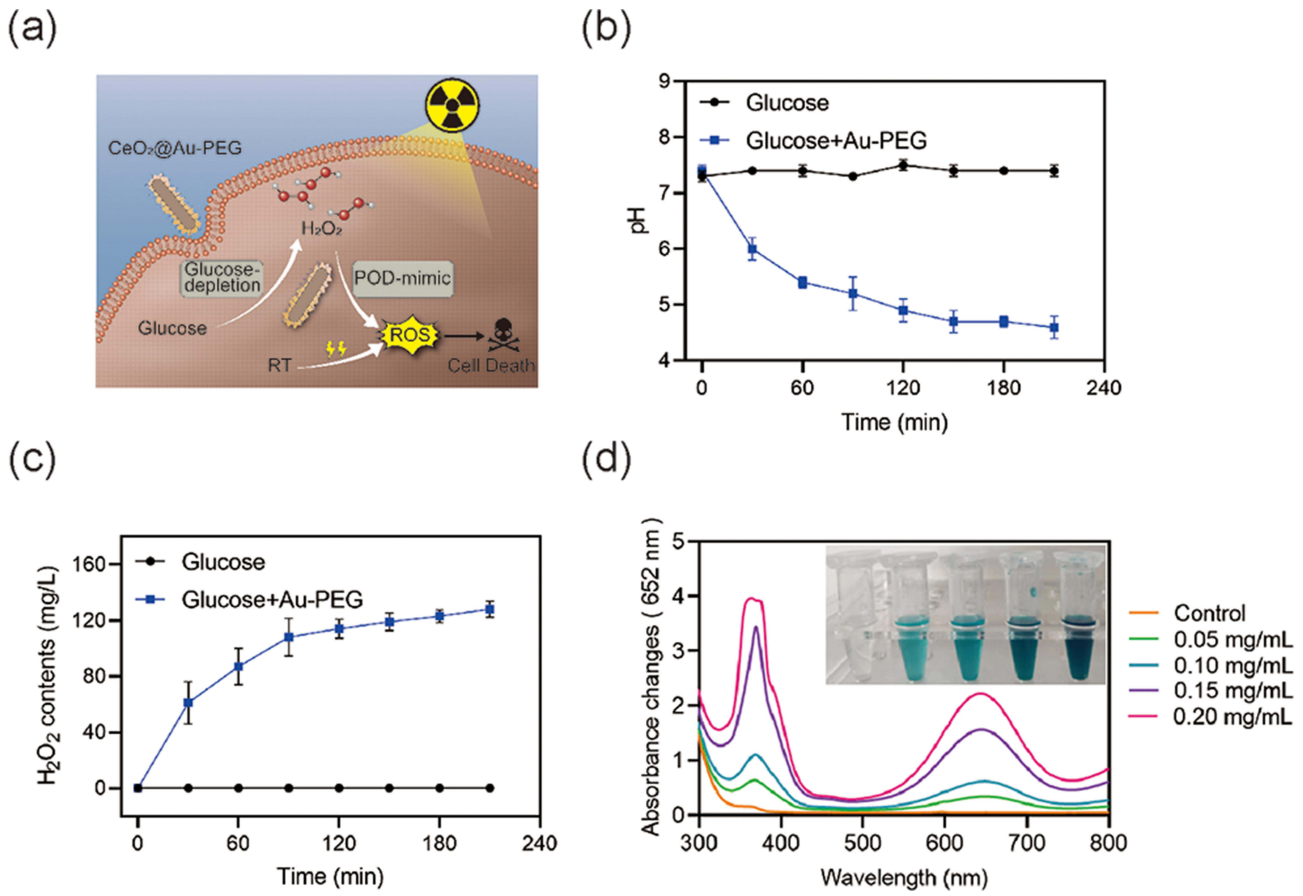

Figure 3 (**a**) Schematic illustration of ROS generation by CeO_2@Au-PEG in cells. (**b** and **c**) Evaluation of oxidation of glucose by measuring pH values and H_2O_2 concentration. (**d**) Evaluation of peroxidase-like activities of various CeO_2@Au-PEG concentrations.

Evaluation of the Catalytic Performance of CeO_2@Au-PEG in Cancer Cells

Inspired by the above results, we further evaluated the antitumor effects of CeO_2@Au-PEG in vitro. Before the application of CeO_2@Au-PEG to cancer cells, it was necessary to confirm its biocompatibility. Cytotoxicity of CeO_2@Au-PEG was tested at various concentrations on tubular epithelial cells (TECs) and murine renal adenocarcinoma RENCA cells. As shown in Figure 4a, no obvious decrease of cell viability was observed in both cell lines. And over 80% cells survived at a concentration of 200 μg/mL. After PEGylation, Cy 5 labeled-CeO_2@Au-PEG exhibited rapid cellular uptake 1 h after co-incubation

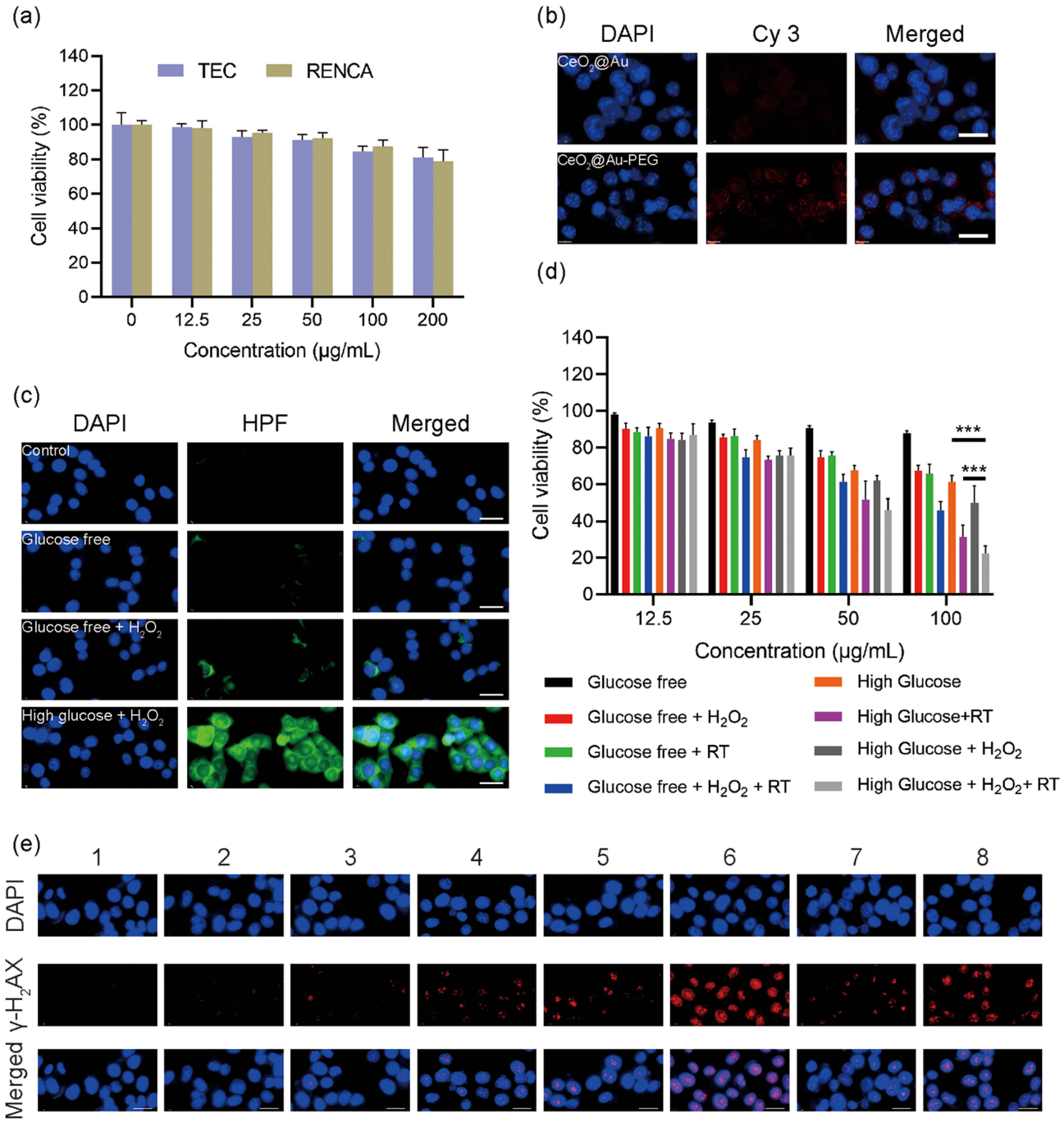

Figure 4 (**a**) Viability of TEC and RENCA cells pre-treated with CeO_2@Au-PEG. (**b**) Cellular uptake of Cy 5 labeled CeO_2@Au or CeO_2@Au-PEG by RENCA cells (Scale bar: 50 μm). (**c**) Confocal fluorescence images showing ·OH generation in RENCA cells treated with CeO_2@Au-PEG at various concentrations using HPF probe (green) (Scale bar: 50 μm). (**d**) Viability of RENCA cells measured by CCK8 assay after various treatments (Scale bar: 50 μm). (**e**) DNA damage assessment by γ-H_2AX staining (Scale bar: 20 μm; group 1: Glucose free, group 2: Glucose free+H_2O_2, group 3: Glucose free+RT, group 4: Glucose free+H_2O_2+RT, group 5:High glucose, group 6: High glucose+RT, group 7: High glucose+H_2O_2, group 8: High glucose+H_2O_2+RT). *** $p < 0.001$. Statistical analyses were conducted using *t*-test.

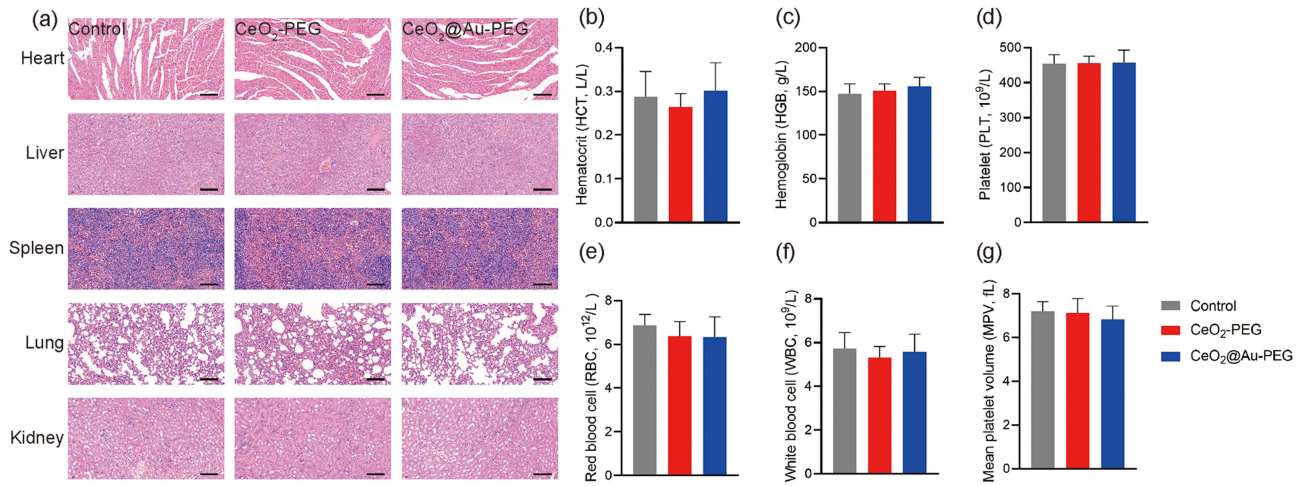

Figure 5 (**a**) H&E staining of excised organ tissues post injection of saline, CeO_2-PEG or CeO_2@Au-PEG NPs (Scale bar: 50 μm). (**b-g**) Blood routine analysis of mice under different treatment.

(Figure 4b). Moreover, the efficacy of RT was enhanced by CeO_2@Au-PEG in vitro. To investigate the amount of ·OH produced during this process, ROS-staining was conducted using HPF probes. As shown in Figure 4c, no apparent green fluorescence was observed in both the control and glucose free groups while a weak fluorescence was seen in the glucose free + H_2O_2 group, which could be attributed to the POD-mimicking property of CeO_2@Au-PEG. On the contrary, a significantly high level of ROS was detected in the high glucose + H_2O_2 group, which was generated from the cascade catalytical reaction mediated by CeO_2@Au-PEG. Next, to validate the dual-catalytic activities on cells, 8 treatment groups were established, including glucose free, glucose free + H_2O_2, glucose free + RT, glucose free + H_2O_2 + RT, high glucose, high glucose + H_2O_2, high glucose + RT and high glucose + H_2O_2 + RT (Figure 4c). It can be seen that in the absence of glucose, CeO_2@Au-PEG showed a weak toxicity on RENCA cells. After the introduction of H_2O_2, there was a decrease in cell survival due to the POD-catalytic activity of CeO_2@Au-PEG. In addition, cell viability was lower upon exposure to RT. The survival rate of cells in the glucose free + H_2O_2 + RT group decreased to 45.7% due to the therapeutic damage mediated by ·OH generation and ionizing irradiation. Cells treated with high glucose only exhibited suppression due to ROS generation from CeO_2@Au-PEG mediated POD-mimicking process. When adding H_2O_2, a decreasing in cell viability was observed thanks to outstanding POD-like property of CeO_2@Au-PEG. A slightly higher cell death was caused by high glucose + H_2O_2 + RT group than high glucose + RT group, which was due to the fact that the H_2O_2 level in mimicking tumor microenvironment was relatively low. In addition, with the addition of glucose and H_2O_2, CeO_2@Au-PEG suppressed the tumor cells, which was likely due to the ROS involved in cascade reaction of glucose oxidase and H_2O_2 depletion. Over 70% of RENCA cells were not viable in the high glucose + H_2O_2 + RT group. Compared with the glucose free + H_2O_2 + RT group, the presence of glucose greatly elevated the cytotoxicity of the nanocomposite. Furthermore, DNA damage post various treatments was assessed by γ-H_2AX staining (Figure 4e). Consistent with the result of CCK 8 assay, the most apparent red fluorescence was observed in the group treated with high glucose + H_2O_2 + RT, suggesting the most severe DNA damage in this group. Further investigation of the expression of caspase 3 in various group confirm the apparent cell apoptosis in CeO_2@Au-PEG enhanced RT in glucose and H_2O_2 situation (Figures S6). Collectively, the above results indicated that CeO_2@Au-PEG was capable of catalyzing the conversion of intracellular glucose to ROS and decreasing tumor cell survival under RT.

Assessment of in vivo Biocompatibility

To confirm the biosafety of CeO_2-PEG and CeO_2@Au-PEG in vivo, main organs including heart, liver, spleen, lung and kidney of mice injected with saline, CeO_2-PEG or CeO_2@Au-PEG were analyzed by hematoxylin and eosin (H&E) staining (Figure 5a). No apparent lesions were observed in mice administrated with CeO_2-PEG or CeO_2@Au-PEG. Blood routine analysis of parameters including hematocrit (HCT), hemoglobin (HGB), platelet (PLT), red blood cell (RBC), white blood cell (WBC) and mean platelet volume (MPV) in Figure 5c-g demonstrated that blood samples from mice administrated with CeO_2-PEG or

CeO_2@Au-PEG were close to the values in the control group. These comprehensive results demonstrated that CeO_2-PEG and CeO_2@Au-PEG had good biocompatibility in vivo.

In vivo Efficacy of CeO_2@Au-PEG in a Mouse Model of Renal Cancer

To verify the anti-renal tumor efficacy of CeO_2@Au-PEG in combination with radiotherapy, subcutaneous tumors were established in BALB/c mice. First of all, biodistribution of CeO_2@Au-PEG in mice post injection via tail vein was analyzed. As shown in Figure S6, most apparent fluorescence intensity was detected in tumor region at 12 h post injection. Four groups were set up including the control, RT, CeO_2@Au-PEG and CeO_2@Au-PEG + RT groups. Tumor volume and body weight in each group were measured every 3 days and mice were executed on day 16 post treatment. As shown in Figure 6a and b, tumor volume in the group treated with PBS showed significant increase with time. Apparent tumor suppression was observed in the group treated with CeO_2@Au-PEG, thus proving the cascade catalytical reaction mediated by CeO_2@Au-PEG. However, therapeutic efficacy of either RT or CeO_2@Au-PEG alone failed to meet the demand for strong tumor inhibition. By striking contrast, the application of CeO_2@Au-PEG + RT dramatically impeded the tumor growth. Besides, by the end of tumor growth monitoring, tumor volume in the control group and RT

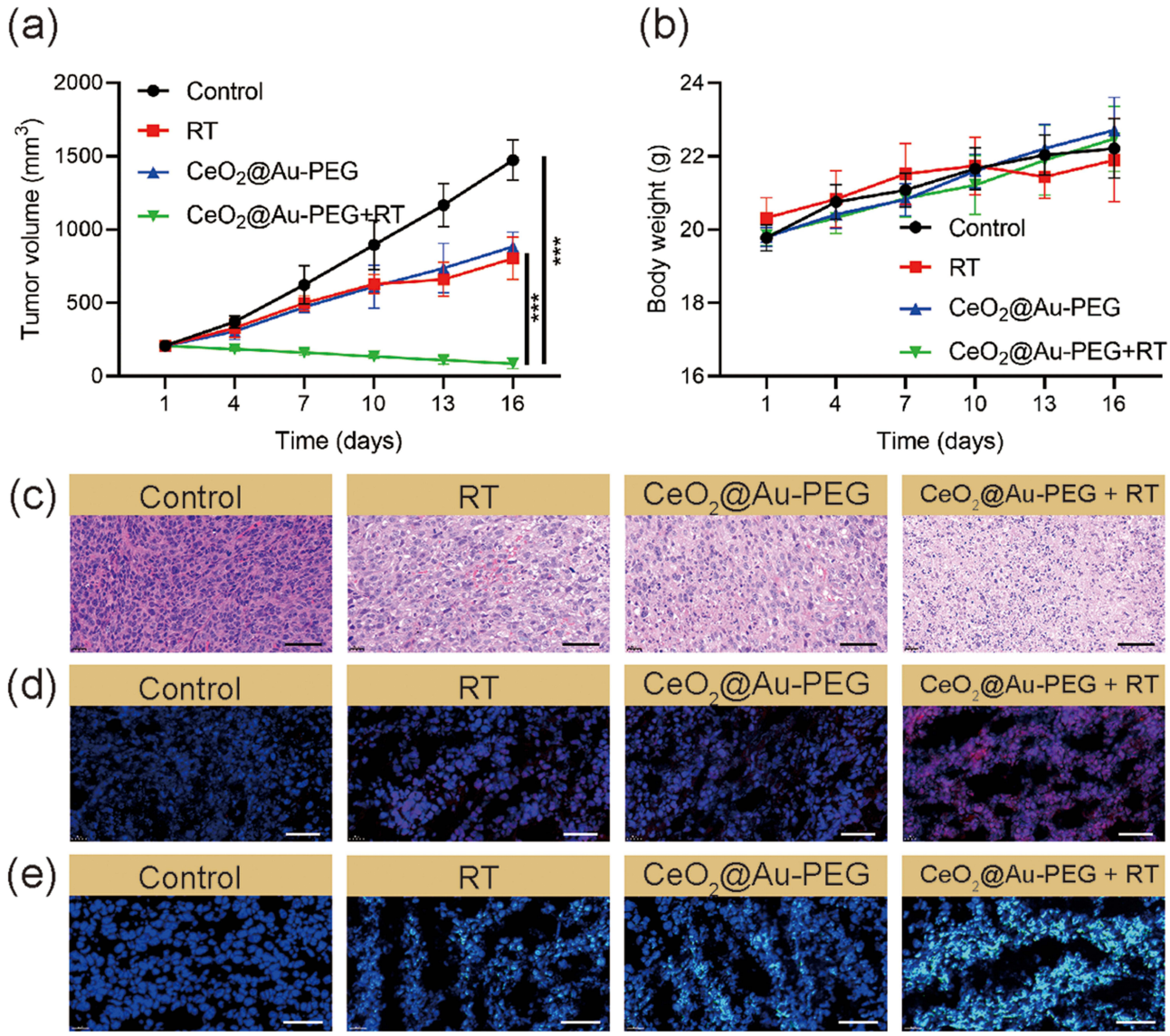

Figure 6 (**a**) The tumor growth curves and (**b**) body weight change curves during different treatments (n = 5). (**c–e**) H&E staining and dihydroethidium (DHE) staining and DCFH-DA staining of tumor tissues after various treatments (Scale bar: 50 μm). *** $p < 0.001$. Statistical analyses were conducted using *t*-test.

group was 5 times and 3 times higher than that in the CeO_2@Au-PEG group, respectively. The image of tumors in four groups in Figure S7 further confirmed the results. There was no significant difference in the body weight of mice body among the four groups.

The in vivo effects of different treatments were evaluated by H&E staining and dihydroethidium (DHE) staining of the tumors. As shown in Figure 6c, moderate cell damages were observed in the RT group and CeO_2@Au-PEG group compared with the control group. H&E images demonstrated severe injuries in the CeO_2@Au-PEG + RT group. Consistent with the H&E staining results, the CeO_2@Au-PEG + RT group showed the brightest red fluorescence which was positively correlated to the amount of superoxide anion ($O_2^{\bullet -}$). Meanwhile, green fluorescence representing hydroxyl radicals (•OH) further confirmed the generation of ROS by CeO_2@Au-PEG + RT in vivo.

Conclusion

In conclusion, a novel CeO_2@Au-PEG nanocomposite with dual-catalytic activities was synthesized to enhance the anti-tumor efficacy of RT in a mouse model of renal cancer. On one hand, CeO_2@Au-PEG could convert glucose in tumor cells into gluconic acid and H_2O_2, due to its ability to oxidize glucose, cutting off the main source of energy to the cancer cells. On the other hand, the resultant H_2O_2 generated in this process was then decomposed into cytotoxic ·OH, causing cell damage. Moreover, composed of two noble elements, CeO_2@Au-PEG enhanced the therapeutic efficacy of RT, leading to stronger anti-tumor effects. CeO_2@Au-PEG showed great biocompatibility both in vitro and in vivo. After treating renal tumor bearing mice with CeO_2@Au-PEG, the tumor cells internalized it, leading to a series of chain reactions which generated a large amount of ROS. Meanwhile, CeO_2@Au-PEG amplified the therapeutic effects of RT. The tumor volume shrank remarkably in the group that received the combination of CeO_2@Au-PEG + RT. In summary, our work provides a novel strategy to treat renal tumors via cascade reaction and radiosensitization mediated by CeO_2@Au-PEG nanocomposite.

Acknowledgment

All animal procedures were performed in accordance with the protocol approved by the Ethics Committee of Laboratory Animal of Henan Provincial Chest Hospital ((Document No. 04-04 of 2021, Animal Ethics Committee). All animal experiments were in accordance with the animal ethics guidelines of the Animal Care and Use Committee of the Laboratory Animal Science Department of Henan Provincial Chest Hospital.

Author Contributions

All authors made a significant contribution to the work reported, whether that is in the conception, study design, execution, acquisition of data, analysis and interpretation, or in all these areas; took part in drafting, revising or critically reviewing the article; gave final approval of the version to be published; have agreed on the journal to which the article has been submitted; and agree to be accountable for all aspects of the work.

Funding

This research was funded by Joint Project of Medical Science and Technology of Henan Province (No. LHGJ20220842).

Disclosure

The authors declare no conflict of interest.

References

1. Siegel RL, Miller KD, Wagle NS, Jemal A. Cancer statistics, 2023. *CA Cancer J Clin*. 2023;73(1):17–48. doi:10.3322/caac.21763
2. Dinges SS, Hohm A, Vandergrift LA, et al. Cancer metabolomic markers in urine: evidence, techniques and recommendations. *Nat Rev Urol*. 2019;16(6):339–362. doi:10.1038/s41585-019-0185-3
3. Andrews JR, Atwell T, Schmit G, et al. Oncologic outcomes following partial nephrectomy and percutaneous ablation for cT1 renal masses. *Eur Urol*. 2019;76(2):244–251. doi:10.1016/j.eururo.2019.04.026
4. Bravi CA, Larcher A, Capitanio U, et al. Perioperative outcomes of open, laparoscopic, and robotic partial nephrectomy: a prospective multicenter observational study (The RECORd 2 Project). *Eur Urol Focus*. 2021;7(2):390–396. doi:10.1016/j.euf.2019.10.013
5. Richters A, Aben KKH, Kiemeney LALM. The global burden of urinary bladder cancer: an update. *World J Urol*. 2020;38(8):1895–1904. doi:10.1007/s00345-019-02984-4

6. Obradovic A, Chowdhury N, Haake SM, et al. Single-cell protein activity analysis identifies recurrence-associated renal tumor macrophages. *Cell*. 2021;184(11):2988–3005.e16. doi:10.1016/j.cell.2021.04.038
7. Campbell Steven C, Uzzo Robert G, Karam Jose A, Chang Sam S, Clark Peter E, Souter L. Renal mass and localized renal cancer: evaluation, management, and follow-up: AUA guideline: part II. *J Urol*. 2021;206(2):209–218. doi:10.1097/JU.0000000000001912
8. Pan W-L, Tan Y, Meng W, et al. Microenvironment-driven sequential ferroptosis, photodynamic therapy, and chemotherapy for targeted breast cancer therapy by a cancer-cell-membrane-coated nanoscale metal-organic framework. *Biomaterials*. 2022;283:121449. doi:10.1016/j.biomaterials.2022.121449
9. Wang M, Chang M, Li C, et al. Tumor-microenvironment-activated reactive oxygen species amplifier for enzymatic cascade cancer starvation/chemodynamic /immunotherapy. *Adv Mater*. 2022;34(4):2106010. doi:10.1002/adma.202106010
10. Zhu Y, Wang W, Cheng J, et al. Stimuli-responsive manganese single-atom nanozyme for tumor therapy via integrated cascade reactions. *Angew Chem Int Ed Engl*. 2021;60(17):9480–9488. doi:10.1002/anie.202017152
11. Jiang C, He T, Tang Q, et al. Nanozyme catalyzed cascade reaction for enhanced chemodynamic therapy of low-H2O2 tumor. *Appl Mater Today*. 2022;26:101357. doi:10.1016/j.apmt.2021.101357
12. Zhen W, Liu Y, Wang W, et al. Specific "unlocking" of a nanozyme-based butterfly effect to break the evolutionary fitness of chaotic tumors. *Angew Chem Int Ed Engl*. 2020;59(24):9491–9497. doi:10.1002/anie.201916142
13. Wang M, Wang D, Chen Q, Li C, Li Z, Lin J. Recent advances in glucose-oxidase-based nanocomposites for tumor therapy. *Small*. 2019;15(51):1903895. doi:10.1002/smll.201903895
14. Fang C, Deng Z, Cao G, et al. Co–ferrocene MOF/glucose oxidase as cascade nanozyme for effective tumor therapy. *Adv Funct Mater*. 2020;30(16):1910085. doi:10.1002/adfm.201910085
15. Wang M, Chang M, Zheng P, et al. A noble AuPtAg-GOx nanozyme for synergistic tumor immunotherapy induced by starvation therapy-augmented mild photothermal therapy. *Adv Sci*. 2022;9(31):2202332. doi:10.1002/advs.202202332
16. Zhang J, Liang C, Wei Z, et al. TME-triggered MnSiO3@Met@GOx nanosystem for ATP dual-inhibited starvation/chemodynamic synergistic therapy. *Biomaterials*. 2022;287:121682. doi:10.1016/j.biomaterials.2022.121682
17. Li C, Wan Y, Zhang Y, et al. In situ sprayed starvation/chemodynamic therapeutic gel for post-surgical treatment of IDH1 (R132H) glioma. *Adv Mater*. 2022;34(5):2103980. doi:10.1002/adma.202103980
18. Xu B, Cui Y, Wang W, et al. Immunomodulation-enhanced nanozyme-based tumor catalytic therapy. *Adv Mater*. 2020;32(33):2003563. doi:10.1002/adma.202003563
19. Cong C, He Y, Zhao S, et al. Diagnostic and therapeutic nanoenzymes for enhanced chemotherapy and photodynamic therapy. *J Mater Chem B*. 2021;9(18):3925–3934. doi:10.1039/D0TB02791J
20. Hua Y, Huang J-H, Shao Z-H, et al. Composition-dependent enzyme mimicking activity and radiosensitizing effect of bimetallic clusters to modulate tumor hypoxia for enhanced cancer therapy. *Adv Mater*. 2022;n/a(n/a):2203734. doi:10.1002/adma.202203734
21. Yu Z, Lou R, Pan W, Li N, Tang B. Nanoenzymes in disease diagnosis and therapy. *Chem Comm*. 2020;56(99):15513–15524. doi:10.1039/D0CC05427E
22. Li Z-L, Wu H, Zhu J-Q, et al. Novel strategy for optimized nanocatalytic tumor therapy: from an updated view. *Small Sci*. 2022;2(7):2200024. doi:10.1002/smsc.202200024
23. Zhu D, Ling R, Chen H, et al. Biomimetic copper single-atom nanozyme system for self-enhanced nanocatalytic tumor therapy. *Nano Res*. 2022;15(8):7320–7328. doi:10.1007/s12274-022-4359-6
24. Tang G, He J, Liu J, Yan X, Fan K. Nanozyme for tumor therapy: surface modification matters. *Exploration*. 2021;1(1):75–89. doi:10.1002/EXP.20210005
25. Phan NM, Nguyen TL, Kim J. Nanozyme-based enhanced cancer immunotherapy. *Tissue Eng Regen Med*. 2022;19(2):237–252. doi:10.1007/s13770-022-00430-y
26. Dong C, Dai X, Wang X, et al. A calcium fluoride nanozyme for ultrasound-amplified and Ca2+-overload-enhanced catalytic tumor nanotherapy. *Adv Mater*. 2022;34(43):2205680. doi:10.1002/adma.202205680
27. Liu J, Wang A, Liu S, et al. A titanium nitride nanozyme for pH-responsive and irradiation-enhanced cascade-catalytic tumor therapy. *Angew Chem Int Ed Engl*. 2021;60(48):25328–25338. doi:10.1002/anie.202106750
28. Nan F, Jia Q, Xue X, et al. Iron phthalocyanine-derived nanozyme as dual reactive oxygen species generation accelerator for photothermally enhanced tumor catalytic therapy. *Biomaterials*. 2022;284:121495. doi:10.1016/j.biomaterials.2022.121495
29. Zhou L, Zhao J, Chen Y, et al. MoS2-ALG-Fe/GOx hydrogel with Fenton catalytic activity for combined cancer photothermal, starvation, and chemodynamic therapy. *Colloids Surf B Biointerfaces*. 2020;195:111243. doi:10.1016/j.colsurfb.2020.111243
30. Cheng X, Yong Y, Dai Y, et al. Enhanced radiotherapy using bismuth sulfide nanoagents combined with photo-thermal treatment. *Theranostics*. 2017;7(17):4087–4098. doi:10.7150/thno.20548